Effect of particle properties and light polarization on the plasmonic resonances in metallic nanoparticles

Urcan Guler[1,*] and Rasit Turan[1, 2]

[1] *Department of Physics, Middle East Technical University, Inonu Boulevard, Ankara 06531, Turkey*
[2] *The Center for Solar Energy Research and Applications (GÜNAM), Middle East Technical University, Inonu Boulevard, Ankara 06531, Turkey*
**urcan@metu.edu.tr*

Abstract: The resonance behavior of localized surface plasmons in silver and gold nanoparticles was studied in the visible and near-infrared regions of the electromagnetic spectrum. Arrays of nano-sized gold (Au) and silver (Ag) particles with different properties were produced with electron-beam lithography technique over glass substrates. The effect of the particle size, shape variations, period, thickness, metal type, substrate type and sulfidation were studied via transmission and reflectance measurements. The results are compared with the theoretical calculations based on the DDA simulations performed by software developed in this study. We propose a new intensity modulation technique based on localized surface plasmons in nanoparticles with asymmetric shapes.

OCIS codes: (240.6680) Surface plasmons; (160.4236) Nanomaterials; (160.4760) Optical properties; (260.5740) Resonance; (290.2200) Extinction; (260.3910) Metal optics

References and links

1. M. Faraday, "Experimental relations of gold (and other metals) to light," Philos. Trans. R. Soc. Lond. B Biol. Sci. **147**, 145–181 (1857).
2. J. C. M. Garnett, "Colours in metal glasses and in metallic films," Philos. Trans. R. Soc. Lond. A **203**(359-371), 385–420 (1904).
3. G. Mie, "Beiträge zur optik trüber medien, speziell kolloidaler metallösungen," Ann. Phys. **25**(3), 377–445 (1908).
4. X. Yu-lin, "Electromagnetic scattering by an aggregate of spheres," Appl. Opt. **34**(21), 4573–4588 (1995).
5. K. S. Yee, "Numerical solution of initial boundary value problems involving Maxwell's equations in isotropic media," IEEE Trans. Antenn. Propag. **14**(3), 302–307 (1966).
6. E. M. Purcell, and C. R. Pennypacker, "Scattering and absorption of light by non-spherical dielectric grains," Astrophys. J. **186**, 705–714 (1973).
7. B. T. Draine, "The discrete dipole approximation and its application to interstellar graphite grains," Astrophys. J. **333**, 848–872 (1988).
8. J. Zhao, A. O. Pinchuk, J. M. McMahon, S. Li, L. K. Ausman, A. L. Atkinson, and G. C. Schatz, "Methods for describing the electromagnetic properties of silver and gold nanoparticles," Acc. Chem. Res. **41**(12), 1710–1720 (2008).
9. K. L. Kelly, E. Coronado, L. L. Zhao, and G. C. Schatz, "The optical properties of metal nanoparticles: the influence of size, shape, and dielectric environment," J. Phys. Chem. B **107**(3), 668–677 (2003).
10. A. Penttila, E. Zubko, K. Lumme, K. Muinonen, M. A. Yurkin, B. T. Draine, J. Rahola, A. G. Hoekstra, and Y. Shkuratov, "Comparison between discrete dipole implementations and exact techniques," J. Quant. Spectrosc. Radiat. Transf. **106**(1-3), 417–436 (2007).
11. L. Novotny, and B. Hecht, Principles of nano optics (Cambridge University Press, New York, 2006).
12. W. Gotschy, K. Vonmetz, A. Leitner, and F. R. Aussenegg, "Optical dichroism of lithographically designed silver nanoparticle films," Opt. Lett. **21**(15), 1099–1101 (1996).
13. H. R. Stuart, and D. G. Hall, "Island size effects in nanoparticle-enhanced photodetectors," Appl. Phys. Lett. **73**(26), 3815–3817 (1998).
14. D. M. Schaadt, B. Feng, and E. T. Yu, "Enhanced semiconductor optical absorption via surface plasmon excitation in metal nanoparticles," Appl. Phys. Lett. **86**(6), 063106 (2005).

#121325 - $15.00 USD Received 5 Jan 2010; revised 8 Jul 2010; accepted 14 Jul 2010; published 30 Jul 2010

15. D. Derkacs, S. H. Lim, P. Matheu, W. Mar, and E. T. Yu, "Improved performance of amorphous silicon solar cells via scattering from surface plasmon polaritons in nearby metallic nanoparticles," Appl. Phys. Lett. **89**(9), 093103 (2006).
16. K. Nakayama, K. Tanabe, and H. Atwater, "Surface plasmon enhanced photocurrent in thin GaAs solar cells," Proc. SPIE **7047**, 704708 (2008).
17. A. K. Pradhan, R. B. Konda, H. Mustafa, R. Mundle, O. Bamiduro, U. N. Roy, Y. Cui, and A. Burger, "Surface plasmon resonance in CdSe semiconductor coated with gold nanoparticles," Opt. Express **16**(9), 6202–6208 (2008).
18. C. Hägglund, M. Zäch, and B. Kasemo, "Enhanced charge carrier generation in dye sensitized solar cells by nanoparticle plasmons," Appl. Phys. Lett. **92**(1), 013113 (2008).
19. K. R. Catchpole, and S. Pillai, "Absorption enhancement due to scattering by dipoles into silicon waveguides," J. Appl. Phys. **100**(4), 044504 (2006).
20. S. Pillai, K. R. Catchpole, T. Trupke, and M. A. Green, "Surface plasmon enhanced silicon solar cells," J. Appl. Phys. **101**(9), 093105 (2007).
21. K. R. Catchpole, and A. Polman, "Design principles for particle plasmon enhanced solar cells," Appl. Phys. Lett. **93**(19), 191113 (2008).
22. H. Mertens, and A. Polman, "Plasmon-enhanced erbium luminescence," Appl. Phys. Lett. **89**(21), 211107 (2006).
23. H. Mertens, A. F. Koenderink, and A. Polman, "Plasmon-enhanced luminescence near noble-metal nanospheres: comparison of exact theory and an improved Gersten and Nitzan model," Phys. Rev. B **76**(11), 115123 (2007).
24. J. S. Biteen, D. Pacifici, N. S. Lewis, and H. A. Atwater, "Enhanced radiative emission rate and quantum efficiency in coupled silicon nanocrystal-nanostructured gold emitters," Nano Lett. **5**(9), 1768–1773 (2005).
25. J. S. Biteen, N. S. Lewis, H. A. Atwater, H. Mertens, and A. Polman, "Spectral tuning of plasmon-enhanced silicon quantum dot luminescence," Appl. Phys. Lett. **88**(13), 131109 (2006).
26. M. Fukushima, N. Managaki, M. Fujii, H. Yanagi, and S. Hayashi, "Enhancement of 1.54-μm emission from Er-doped sol-gel SiO_2 films by Au nanoparticles doping," J. Appl. Phys. **98**(2), 024316 (2005).
27. T. D. Corrigan, S. H. Guo, H. Szmacinski, and R. J. Phaneuf, "Systematic study of the size and spacing dependence of Ag nanoparticle enhanced fluorescence using electron-beam lithography," Appl. Phys. Lett. **88**(10), 101112 (2006).
28. K. Tanabe, "Optical radiation efficiencies of metal nanoparticles for optoelectronic applications," Mater. Lett. **61**(23-24), 4573–4575 (2007).
29. H. Garcia, J. Trice, R. Kalyanaraman, and R. Sureshkumar, "Self-consistent determination of plasmonic resonances in ternary nanocomposites," Phys. Rev. B **75**(4), 045439 (2007).
30. J. P. Kottman, O. J. F. Martin, D. R. Smith, and S. Schultz, "Field polarization and polarization charge distributions in plasmon resonant nanoparticles," N. J. Phys. **2**, 27 (2000).
31. S. Zou, and G. C. Schatz, "Generating narrow plasmon resonances from silver nanoparticle arrays: influence of array pattern and particle spacing," Proc. SPIE **5513**, 22–29 (2004).
32. B. T. Draine, and P. J. Flatau, "User guide for the discrete dipole approximation code DDSCAT 7.0," *http://arXiv.org/abs/0809.0337* (2008).
33. M. A. Yurkin, V. P. Maltsev, and A. G. Hoekstra, "The discrete dipole approximation for simulation of light scattering by particles much larger than the wavelength," J. Quant. Spectrosc. Radiat. Transf. **106**(1-3), 546–557 (2007).
34. B. T. Draine, and P. J. Flatau, "Discrete-dipole approximation for scattering calculations," J. Opt. Soc. Am. A **11**(4), 1491–1499 (1994).
35. V. P. Drachev, U. K. Chettiar, A. V. Kildishev, H. K. Yuan, W. Cai, and V. M. Shalaev, "The Ag dielectric function in plasmonic metamaterials," Opt. Express **16**(2), 1186–1195 (2008).
36. C. L. Haynes, A. D. McFarland, L. Zhao, R. P. V. Duyne, G. C. Schatz, L. Gunnarsson, J. Prikulis, B. Kasemo, and M. Kall, "Nanoparticle optics: the importance of radiative dipole coupling in two-dimensional nanoparticle arrays," J. Phys. Chem. B **107**(30), 7337–7342 (2003).
37. L. Zhao, K. L. Kelly, and G. C. Schatz, "The extinction spectra of silver nanoparticle arrays: influence of array structure on plasmon resonance wavelength and width," J. Phys. Chem. B **107**(30), 7343–7350 (2003).
38. A. Moores, and F. Goettmann, "The plasmon band in noble metal nanoparticles: an introduction to theory and applications," N. J. Chem. **30**(8), 1121–1132 (2006).
39. S. J. Norton, and T. V. Dinh, "Spectral bounds on plasmon resonances for Ag and Au prolate and oblate nanospheroids," J. Nanophoton. **2**(1), 029501 (2008).
40. W. Gotschy, K. Vonmetz, A. Leitner, and F. R. Aussenegg, "Thin films by regular patterns of metal nanoparticles: tailoring the optical properties by nanodesign," Appl. Phys. B **63**, 381–384 (1996).
41. S. A. Maier, and H. A. Atwater, "Plasmonics: localization and guiding of electromagnetic energy in metal/dielectric structures," J. Appl. Phys. **98**(1), 011101 (2005).
42. M. N'Gom, J. Ringnalda, J. F. Mansfield, A. Agarwal, N. Kotov, N. J. Zaluzec, and T. B. Norris, "Single particle plasmon spectroscopy of silver nanowires and gold nanorods," Nano Lett. **8**(10), 3200–3204 (2008).
43. A. V. Zayats, I. I. Smolyaninov, and A. A. Maradudin, "Nano-optics of surface plasmon polaritons," Phys. Rep. **408**(3-4), 131–314 (2005).
44. T. W. Ebbesen, H. J. Lezec, H. F. Ghaemi, T. Thio, and T. A. Wolff, "Extraordinary optical transmission through sub-wavelength hole arrays," Nature **391**(6668), 667–669 (1998).

#121325 - $15.00 USD Received 5 Jan 2010; revised 8 Jul 2010; accepted 14 Jul 2010; published 30 Jul 2010

45. J. D. Jackson, Classical Electrodynamics (John Wiley 1998), 3rd ed.
46. M. D. McMahon, R. Lopez, H. M. Meyer III, L. C. Feldman, and R. F. Haglund, Jr., "Rapid tarnishing of silver nanoparticles in ambient laboratory air," Appl. Phys. B **80**(7), 915–921 (2005).
47. W. Cao, and H. E. Elsayed-Ali, "Stability of Ag nanoparticles fabricated by electron beam lithography," Mater. Lett. **63**(26), 2263–2266 (2009).

1. Introduction

Unusual characteristics of light interaction with metal nanoparticles were noticed at the early stages of modern civilization and used in architectural applications without knowledge of the underlying physical basis. Although metal nanoparticles dispersed in glass were studied beginning in the 19th century, a deeper understanding of the physical mechanism was provided by the pioneering study of Gustav Mie in 1908, in which the solutions of the Maxwell equations for particles with spherical symmetry were presented [1–3]. His approach has been used as a guide in the majority of the studies in the field of plasmonics and has also been improved for the cases in which clusters of spherical particles are employed [4]. Though analytical solutions to the problem are invaluable, the inability to describe systems with asymmetries presents a demand for numerical approximations. In the second half of the 20th century, methods based on different approaches were developed and widely used to predict the optical behavior of nano-sized particles with several different geometries [5–10].

When metal particles with sizes smaller than the wavelength of incident radiation are illuminated, electrons occupying the conduction band are driven by the applied electromagnetic field. The time harmonic motion of electrons in the nanoparticle results in polarization, which in turn causes a restoring force and leads to an oscillation with characteristics dependent on the material properties and geometry. Incident radiation having frequencies at the resonance condition of the oscillator leads to localized surface plasmon resonances (LSPR), which result in strong interaction of light with the nanoparticle. The nature of the interaction, whether it is absorption or scattering, is mainly dependent on the material and size of the particle. Cross sections for absorption and scattering for a particle smaller than the wavelength of illumination are given as,

$$C_{abs} = \frac{k}{\varepsilon_o}\mathrm{Im}\left[\alpha(\omega)\right] \tag{1.a}$$

$$C_{sca} = \frac{k^4}{6\pi\varepsilon_o^{\,2}}\left|\alpha(\omega)\right|^2. \tag{1.b}$$

Equations (1.a) and (1.b) show that both cross sections are dependent on the polarizability of the particle, which is proportional to the size of the particle with R^3 [11]. Thus, as the particle size increases, re-radiation of the energy by the particle to the surrounding medium is expected to be dominant. For the case of particles with relatively smaller dimensions, the dissipation of the energy within the particle is more likely.

Although it was possible to produce nano-sized metal particles even in the earliest studies, the ability to control the shape, size and order of the nanoparticles was possible only after the development of lithographical techniques [12]. However, it is hardly possible to pattern features with the desired dimensions by conventional optical lithography, which is limited by the wavelength of the light source used. Conversely, the electron-beam lithography technique, which takes advantage of the relatively shorter wavelengths of electrons and the more efficient focusing behavior, provides an excellent tool to form patterns with nanoparticles with dimensions less than 100 nm.

The improvement of nanomanufacturing techniques gave rise to extensive studies over the last decade. Many studies investigating the effect of metal nanoparticles on the performance enhancement of semiconductor optoelectronic devices such as solar cells can be found in the literature. Stuart and Hall studied the effect of metal nanoparticle size on the photocurrent

#121325 - $15.00 USD Received 5 Jan 2010; revised 8 Jul 2010; accepted 14 Jul 2010; published 30 Jul 2010

enhancement in photodetectors, resulting in an enhancement factor of 18 by the deposition of silver nanoparticles on the photodetectors [13]. Schaadt et al. reported a 50% to 80% enhancement of the photocurrent response at the resonance frequencies for a Si pn junction diode using ~100 nm gold nanoparticles [14]. Gold nanoparticles have also been found to increase the maximum power output of an a-Si:H pi-n thin film solar cell by 8.3% in a study by Derkacs et al. [15]. The authors also predicted a further enhancement if particle deposition techniques that do not degrade the performance characteristics of the device itself are used. Surface plasmon enhanced photocurrents for GaAs solar cells were studied by Nakayama et al. [16]. The authors examined the behavior of Ag and Al nanoparticles with dimensions between 60 and 150 nm templated on the surface of the solar cell. Smaller nanoparticles having dimensions around 60 nm showed strong absorption and degradation of the device performance while relatively larger particles improved the photocurrent, in agreement with the theory. Pradhan et al. demonstrated the use of gold nanoparticles on a CdSe semiconductor, with an enhancement factor of nine for room-temperature photoluminescence, indicating the strong absorption enhancement via the excitation of surface plasmon resonance in the metallic nanoparticles [17]. The enhancement effects of metallic nanoparticles were also demonstrated for dye-sensitized solar cells by Hägglund et al. [18]. In recent studies, Catchpole et al. systematically examined the factors affecting the performance of plasmonic solar cells [19,20]. They concluded that cylindrical and hemispherical particles lead to a higher performance than spherical particles, and silver gives better optical performance than gold, as should be expected given the extremely low value of the imaginary component of the dielectric constant in silver [21].

Another promising application of nano-sized metal particles is the luminescence enhancement due to plasmonic coupling. The strong polarization dependence of the plasmonic effects and modifications of the decay rates of a dipole emitter coupled to metal nanospheres located nearby were considered by Mertens et al. [22,23]. Furthermore, the signal enhancement obtained from luminescent materials such as Si quantum dots [24,25], Er [26] and fluorophores [27] were experimentally verified.

Studies on localized surface plasmons show that the mechanism is open to engineering due to the large number of material parameters affecting the resultant optical characteristics of the system. Tanabe studied the optical radiation efficiencies of 11 kinds of metal by classical electromagnetic theory [28]. Ag, Al, Au and Cu were found to have higher optical radiation efficiencies. Garcia et al. developed a self-consistent technique to predict the behavior of plasmon resonances in ternary nanocomposites as a function of the wavelength in agreement with experimental data [29]. In a relatively early study, Kottman et al. showed that it is possible to predict the plasmon resonances of metallic nanoparticles with different shapes with numerical techniques taking the polarization of the incident radiation in to the account [30]. Zou et al. showed that, apart from the morphology of the nanoparticles, the pattern of the particle array also plays a significant role in the resonance conditions [31].

In this report, we present the results of our recent studies on the LSPR behavior of Au and Ag nanoparticles engineered by Electron Beam Lithography (EBL). We attempted to reach a comprehensive understanding of this system with all the parametric features that may be of interest to the scientific and technological community working in this field. With this aim, we focused on the transmission, reflection and absorption characteristics of different systems with varying structural properties. First of all, the optical transmittance data of a typical sample produced with EBL was compared to that of a sample produced with the self-assembly method that is believed to be the most suitable technique for mass production. This comparison demonstrates the difference between these systems fabricated and measured in the same laboratory. Then, to reveal the LSPR effect and its dependence on the nanoparticle properties, gold (Au) and silver (Ag) nanoparticles with increasing sizes, periods (lattice constant) and thicknesses were optically examined. The variation with size and thickness was shown to correlate nicely with the theoretical expectations derived from the DDA-based

#121325 - $15.00 USD Received 5 Jan 2010; revised 8 Jul 2010; accepted 14 Jul 2010; published 30 Jul 2010

software that was developed during this study. The extreme cases, in which nanoparticles are small when compared to their period or they touch each other, were examined to understand the transition between these two extremes and the effects of inter-particle interactions.

Though particles are intended to be circular cylinders in shape, deviations from the circular shape were observed due to the astigmatism of the e-beam during the production. In these cases, particles take an elliptical form, which generates resonance peaks consisting of two closely located components, each corresponding to one axis of the ellipsoid. These two components can be monitored independently using radially polarized light along the principle axes of the ellipsoid. We studied this effect in a series of samples with different particle sizes and periods. We showed that the polarization effect can be used in a new type of optical intensity modulator based on plasmonic effects.

It is commonly accepted that Ag nanoparticles have superior scattering properties because they have a more favorable dielectric constant compared to Au nanoparticles. However, the sulfidation of Ag and its degrading effect are generally overlooked. We performed a series of aging experiments with Au and Ag nanoparticles to understand the effects of sulfidation in the air on the LSPR behavior of Ag compared to Au. The degradation of the resonance peak is clearly observed for Ag nanoparticles.

2. Numerical modeling

Modeling the optical behavior of nano-sized metal particles is of great importance due to the promising applications in a wide range of areas. Thus, several numerical techniques have been developed to investigate the interaction of light with particles in complex shapes where analytical solutions cannot be applied. Finite Difference Time Domain (FDTD) and Discrete Dipole Approximation (DDA) methods can be listed as two of the most widely used approaches to the problem. In the DDA method, metal nanoparticles with any shape can be represented as a collection of small polarizable elements ordered in a cubic lattice. One of the advantages of DDA is the availability of free codes developed in different environments such as DDSCAT [32], and ADDA [33]. However, in this work, we have developed our own code following the guidance of the work of Draine et al. To summarize the DDA method used in this work, a cylindrical particle represented by N polarizable elements is taken as an example in the following description. As the particle is illuminated, each element will face an external electric field of the incoming light and the dipole emission from the neighboring N-1 elements. The relative positions of the elements define the shape of the particle, thus taking the retardation and shape effects into account. Obviously, a larger number of polarizable elements is required to obtain more accurate results. However, a higher density of elements requires longer computation times, which are sometimes not practical. To satisfy the condition of small element sizes when compared to the wavelength of incident light and an accurate representation of the particle shape, the following criteria were assigned in earlier studies [34],

$$|m|kd \le 1 \tag{2.a}$$

$$N > (4\pi/3)|m|^3 \left(ka_{eff}\right)^3 \tag{2.b}$$

where ‘m’ is the refractive index of the target, ‘d’ is the lattice spacing between the elements, ‘k’ is the wavenumber of the incident field and ‘ a_{eff} ’ is the effective radius of the target. It is also stated that those criteria have significant effects on the computation of the absorption efficiencies.

In this study, the criteria given above are violated to some extent because the extinction efficiencies are mainly considered. Since particles involved in this work are known to dominantly have scattering, which is less affected by the criteria listed above, the extinction efficiencies provide sufficient data about the effects of several parameters on the resonance

#121325 - $15.00 USD Received 5 Jan 2010; revised 8 Jul 2010; accepted 14 Jul 2010; published 30 Jul 2010

wavelengths. The comparison between the rate of absorption and scattering in a particle will be discussed in the results section below. Two systematic deviations from the experimental results can be identified in the extinction efficiencies calculated by the software: differences in the signal magnitude in the smaller-wavelength regions and 50 nm spectral shifts in the peak positions with respect to the experimental results. The former deviation is due to the violation of Eq. (2.a) because the wavelength of the incident light is small and the lattice spacing between the elements remains constant, 10 nm in our simulations, for a particular computation. However, the latter deviation is due to the inconsistencies of the optical constants for a specific metal [35]. In this study, the dielectric constants of the metals that are employed in the simulations are computed with a multiple-oscillator approach. Thus, small deviations are expected when compared to the real values, which in turn result in systematic shifts in each calculation when compared to the corresponding experimental results. Single metal particles are simulated as if they are located in a homogenous medium with dielectric constants averaged from ITO and air.

3. Experimental

In this work, a CamScan CS3200 scanning electron microscope (SEM) modified with a laser interferometric stage and a pattern generator system was used as an electron-beam lithography system. Most of the nanoparticle arrays were patterned on microscope slides coated with thin indium tin oxide (ITO) layers, while patterns formed on bare slides were also studied. Poly methyl methacrylate (PMMA) was used as an electron beam resist in the production period for all samples and coated with a spin coater at 6000 rpm over the substrate to obtain a layer thickness of approximately 100 nm in a clean-room environment. Following the e-beam exposure and pattern development, thin metal films with varying thicknesses were deposited over the samples with a resistive thermal evaporator system with a growth rate of 0.8 angstrom/sec. Nanoparticle arrays with dimensions of 100 x100 μm^2 were patterned over the substrates, and an optical microscope coupled to an MS257 monochromator was employed to perform the optical characterization.

The samples prepared with the self-assembly method were fabricated by evaporating a thin (5-20 nm) metal film on the desired substrate with thermal evaporation followed by a heat treatment at 500 to 800 °C for 3 hours in nitrogen environment to induce nanoparticle formation.

4. Results

4.1 Electron beam lithography vs. self-assembly

It is clear that EBL is a superior tool for a good control over the geometry of the nano-sized particles when compared with the self-assembly of nanoparticles from a thin film deposited on a substrate. However, while EBL offers more precisely defined nanostructures, which is obviously good for a study for the proof of concept, the self-assembly technique represents a better approach for large-scale applications such as solar cells. It is thus of interest to understand the differences and similarities between the EBL method and the self-assembly growth of metal nanoparticles. Figure 1 shows the SEM images of Au nanoparticles fabricated on a glass substrate by both techniques and their extinction spectra with the characteristic peak associated with the plasmonic resonance induced by the electric field of the incident light beam.

#121325 - $15.00 USD Received 5 Jan 2010; revised 8 Jul 2010; accepted 14 Jul 2010; published 30 Jul 2010

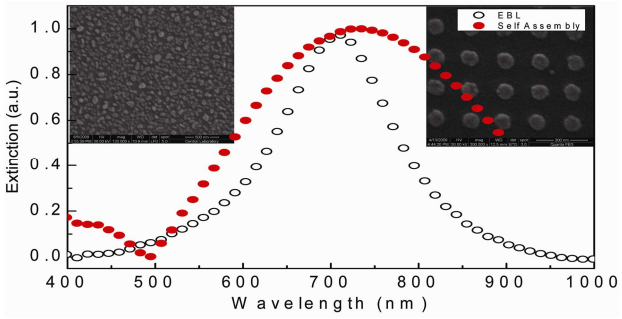

Fig. 1. The extinction spectra (1 – T) and SEM images of two samples produced with self assembly (on the left) and electron beam lithography (on the right) methods.

As seen from the SEM images, Au particles produced with the self-assembly method exhibit large variations in size and shape. In contrast, 90 nm particles patterned with EBL are almost uniquely defined with their circular cylindrical shape and period (see Fig. 1). The resonance condition and the shape of the resonance peak in the extinction spectra are apparently different for the two systems. LSPR peak for particles fabricated with EBL is much narrower than what is observed for the one obtained by the self-assembly method. With diversity in the shape of the particles and sizes varying from a few to a hundred nanometers, the self-assembled structure has a resonance peak so broad that changes in the curve due to geometrical variations cannot be observed easily. However, a correlation between the expected resonance values for the mean particle size as determined from the analysis of the SEM image can be searched. The mean particle size is found to be 120 nm which is expected to generate a resonance peak at around 730 nm by the DDA calculation. This is in agreement with the observed behavior shown in Fig. 1.

4.2. Effect of an indium tin oxide (ITO) layer

A thin conducting layer is commonly applied to prevent the charging effect in EBL when using insulating substrates. On the other hand, conducting oxides such as indium thin oxide (ITO) are useful in optoelectronic applications in which an electrical connection and light transmission are simultaneously needed. As we introduce a different surrounding medium, the effect of the presence of a thin ITO layer on the resonance conditions should be investigated. Two identical arrays consisting of Au nanoparticles with diameters of 140 nm were patterned on bare and ITO-coated microscope slides to compare between these two cases. Figure 2 shows the reflectance spectra for Au nanoparticles with identical geometries patterned over the bare and ITO-coated glass substrates. Though a slight redshift in the resonance peak is expected for the ITO-coated sample due to the higher effective dielectric constant, it is found that the shift cannot be resolved due to the intensity enhancement in the ITO-coated substrate. Similarly, the slight broadening of the peak expected due to the conducting nature of ITO is not detectable. The increase in the reflectance intensity is the major difference observed in the case of the ITO-coated sample. Such an increase in the reflectance can be attributed to the fact that scattered light from the Au nanoparticles undergoes a Fresnel reflection at the ITO/glass interface, which is further enhanced due to the angle of incidence gained after scattering from the Au particles.

#121325 - $15.00 USD Received 5 Jan 2010; revised 8 Jul 2010; accepted 14 Jul 2010; published 30 Jul 2010

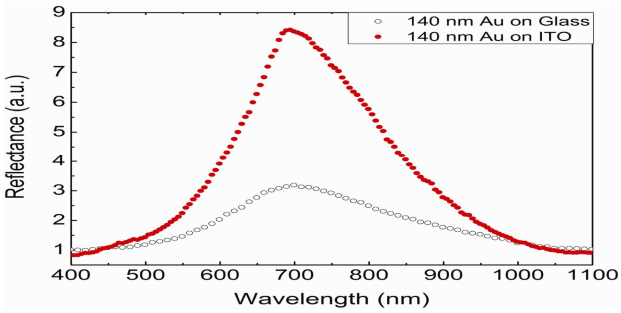

Fig. 2. The reflectance data of Au nanoparticles patterned over glass substrates w/o an ITO layer (20 nm).

4.3 Effect of size, shape and period

In this section, geometrical parameters affecting the resonance characteristics are discussed experimentally and theoretically. Ag and Au nanoparticles are widely preferred in studies on plasmonic applications due to the optical performance and long-term stability of these materials, respectively. Increasing sizes of nanoparticles are commonly known to cause redshifts and the broadening of the resonance peak. Figure 3 shows the reflectance spectra obtained from arrays of Au nanoparticles with sizes varying from 60 to 145 nm and lattice constants kept constant. The figure verifies the redshift and broadening in the peak when the particle sizes increase. Furthermore, the increasing intensity in the reflectance peaks is obviously due to the larger surface coverage of the arrays with larger particles but the same lattice constants. For this set of samples, the fabricated particles were slightly ellipsoidal due to the astigmatism effect of the e-beam lithography system. Thus, under unpolarized illumination, oscillations corresponding to each principal axis of the ellipsoids contribute to the resonances, and thus broader peaks are observed.

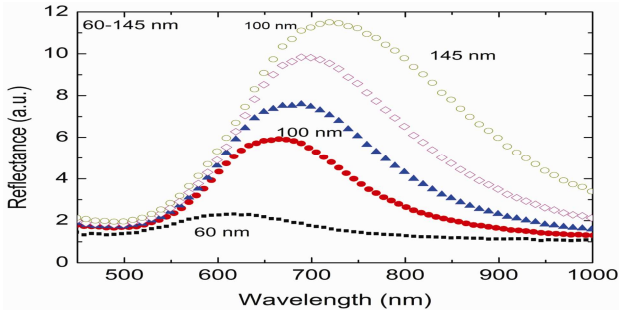

Fig. 3. Au nanoparticle arrays with a lattice constant of 200 nm patterned over ITO-coated glass. The nanoparticle thicknesses are 20 nm, and diameters vary between 60 and 145 nm.

To investigate the variations in the shape of the nanoparticles and to reveal the contributions from each axis of the ellipsoids to the resonance peak, nanoparticles were illuminated with linearly polarized light parallel to the axes. The reflection spectrum obtained by linearly polarized and unpolarized light from Au ellipsoidal cylinders with axes 80 & 110 nm are plotted in Fig. 4. The SEM image of the same sample is also displayed in the figure. It is seen that the resonance peaks corresponding to the two axes of the ellipsoids are easily resolved by polarized illumination and found to be located near 630 and 730 nm. The broader resonance peaks measured in the self-assembled sample, which has a larger variation in its shape and inter-particle distance, is better understood from this result. The sensitivity of the resonance peak position to the slight variation in the particle geometry is also confirmed by the DDA calculation theoretically. This high sensitivity may lead to new applications like intensity modulation by plasmonic oscillations, as described in Section 4.6.

#121325 - $15.00 USD Received 5 Jan 2010; revised 8 Jul 2010; accepted 14 Jul 2010; published 30 Jul 2010

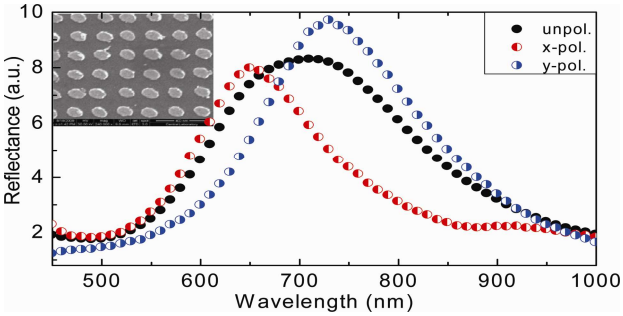

Fig. 4. The reflectance spectra of ellipsoidal Au nanoparticles with axes of 80 and 110 nm, with lattice constant of 200 nm over ITO coated glass. Particle array is observed under unpolarized illumination and linear polarizations parallel to short (x-pol) and large (y-pol) axes. The inset gives SEM images of the corresponding ellipsoid nanoparticle array.

The position and the width of the resonance peak should also be affected by the interaction of neighboring particles. It is therefore plausible to consider the effect of inter-particle interactions on the resonance properties. Figure 5(a) presents the reflectance spectra for particles with sizes between 55 and 110 nm and a lattice constant of 300 nm standing over a glass substrate with a 20 nm ITO coating. Having all the parameters similar to the previous sample except for the inter-particle separation, the reflectance spectra of this set of samples exhibit separate peaks corresponding to principle axes of the ellipsoid. The peaks can be resolved even under unpolarized illumination in this case because the particles are sufficiently far away from each other. Although ellipsoidal Au nanoparticles with axes dimensions of 70 and 110 nm gives resonance peaks at almost the identical position as those given in Fig. 4 (with axes of 80 and 110), two important differences can be identified. Apart from the decrease in the reflectance intensity, which is directly related to the reduced surface coverage in this case, the shape of the peak under the unpolarized illumination differs from the former case due to the reduced coupling among the particles. The larger separation between particles reduces the coupling and allows distinct peaks to be observed without using polarized light. However, when the particle size is reduced, the relative difference between the axes is reduced too. This, along with the intensity reduction due to less surface coverage, results in broader peaks with indistinguishable components for smaller particles.

In order to verify the experimental observations, DDA simulations were performed for a single Au nanoparticle with ellipsoidal geometry with the given dimensions. The typical behavior with separate resonance peaks corresponding to distinct axes can be obtained as shown in Fig. 5(b), where the extinction efficiency of a 20 nm thick Au nanoparticle with axes of 80 and 110 nm located on an ITO/Air interface is plotted as a function of the wavelength for an unpolarized-light illumination. The DDA results confirm the presence of two distinct resonance peaks when there is no coupling between neighboring particles. The slight deviation in the simulation results for shorter wavelengths is due to the relatively larger polarizable elements used in the calculations to reduce the computation time to manageable values. The precision of the calculation worsens for shorter wavelength because the ratio of the wavelength to the polarizable element dimensions reduces. Nevertheless, the results are still accurate enough to provide a rigorous explanation for the experimental observation.

#121325 - $15.00 USD Received 5 Jan 2010; revised 8 Jul 2010; accepted 14 Jul 2010; published 30 Jul 2010

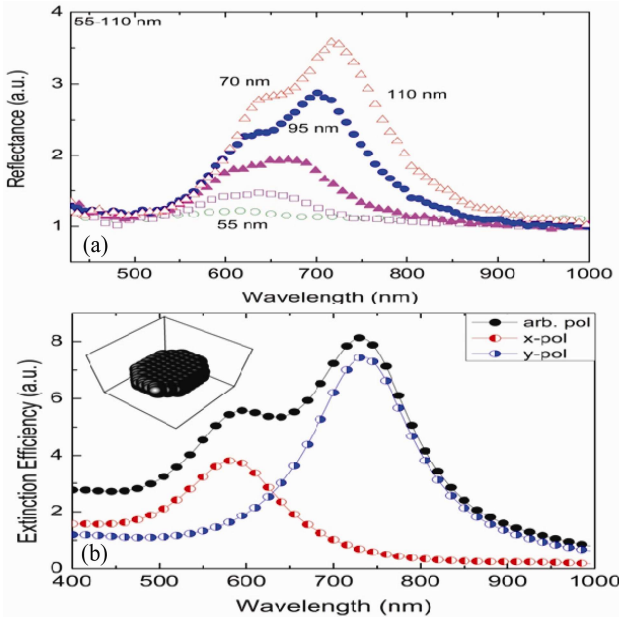

Fig. 5. (a) Reflectance spectra of Au nanoparticle arrays with 300 nm lattice constant and varying dimensions located over ITO coated microscope slide. Ellipsoidal shapes of nanoparticles induce distinct peaks under unpolarized illumination. (b) DDA simulation results for the extinction efficiency of a single Au nanoparticle with 80 and 110 nm axes standing on ITO/Air interface.

The effect of particle interaction and its variation with an increasing lattice constant can easily be observed from a comparison of the resonance peaks in the reflectance spectra of particles with identical shapes and dimensions but varying inter-particle distances. The reflectance spectra of arrays with increasing periods are given in Fig. 6, where the illumination with linear polarization parallel to the long axis is considered. As the lattice constants of the arrays are increased, a narrowing in the width of the resonance peaks is observed clearly from the FWHM measurements given in the figure. These results clarify the existence of distinct peaks in the reflectance spectra of samples with a 300 nm period; whereas a single, broad peak appears for the case of the 200 nm particle separation. Another feature seen upon the comparison of the samples with varying lattice constants is the slight redshift occurring in the peak position as the separation of the particles increases, which again can be attributed to inter-particle coupling among neighboring particles.

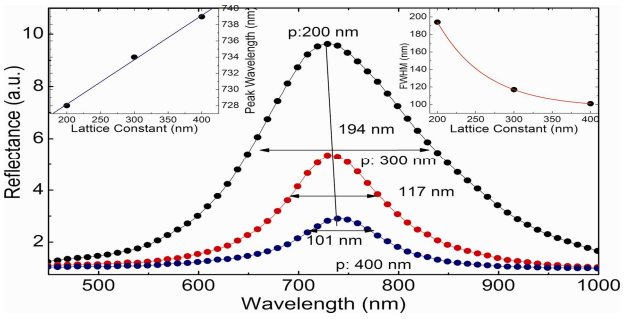

Fig. 6. The reflectance spectra of arrays with the same ellipsoidal nanoparticle sizes, 80-110 nm, but varying lattice constants from 200 to 400 nm, under illumination polarized parallel to the long axis. Increasing the inter-particle distance results in redshift of the peak position and narrowing of the width.

#121325 - $15.00 USD Received 5 Jan 2010; revised 8 Jul 2010; accepted 14 Jul 2010; published 30 Jul 2010

In earlier studies, electromagnetic interactions among neighboring metal nanoparticles were shown to have two different components, the electrostatic and electrodynamic terms. The electrostatic term, which is proportional to $1/r^3$, is found to be dominant for small inter-particle separations and to cause blue-shifts in the resonance peak as the lattice constant increases. On the other hand, the electrodynamic term, being proportional to 1/r, was shown to dominate when the lattice constant of the array is large and to cause red-shifts in the resonance peak and reduce FWHM as the inter-particle distance is increased [36,37]. The lattice constants discussed in our study are comparable to the wavelength of the incident light, and reflectance measurements agree well with the expected behavior. The insets in Fig. 6 show the relationship between the peak wavelength (left) and FWHM (right) with the lattice constants of the arrays. The resonance peak is observed to be almost linearly proportional to the inter-particle distance, r, as expected. On the other hand, the FWHM of the peak is observed to have an inverse relationship with the parameter, r, in the large-separation regime. Although an exponential function can be fitted to the FWHM data the number of data points is not sufficient to reach conclusions about this relationship.

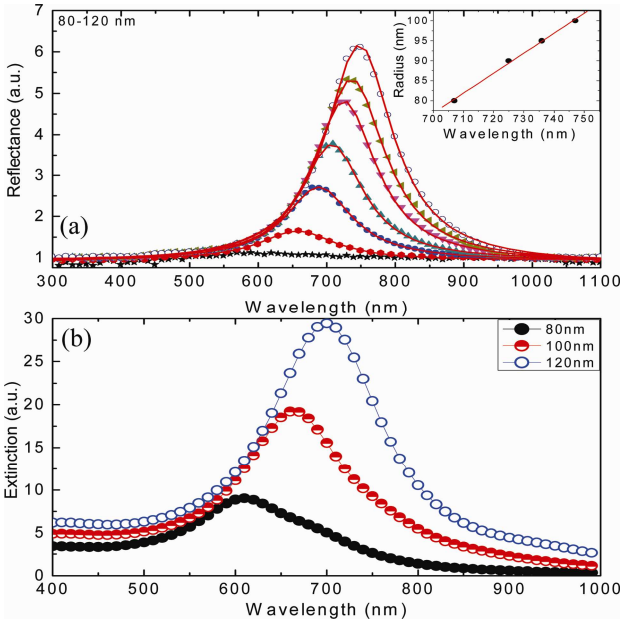

Fig. 7. (a) The LSPR peaks obtained from ellipsoidal cylinders with axis dimensions increasing from 80 to 120 nm under illumination linearly polarized parallel to the long axis. The peaks are found to be Lorentzian with accuracy better than 99%, illustrating the validity of Lorentz-Drude model to describe real metals. (b) The extinction efficiency of particles located on ITO/air boundary with dimensions of 80, 100 and 120 nm calculated with DDA method.

In order to further examine the LSPR peaks, ellipsoidal metal nanoparticles with increasing sizes were illuminated with linearly polarized light with the electric field component parallel to the larger axes. The redshift and broadening of the resonance peak and an increase in the reflectance intensity were observed as predicted by the theory. Furthermore, the resonance peaks were found to be Lorentzian in shape, which is known to be the solution of the problem of a forced and damped oscillator. Each peak corresponding to particles with varying axis dimensions between 80 and 120 nm was found to be Lorentzian with accuracy better than 99%. The reflectance spectra of the nanoparticles illuminated with linearly polarized light are shown in Fig. 7(a). These results verify the Lorentzian expression for the scattering cross section of a metal nanoparticle along with the nearly linear real dielectric constant of Au in the region of interest [38,39]. Furthermore, the redshift in the central

#121325 - $15.00 USD Received 5 Jan 2010; revised 8 Jul 2010; accepted 14 Jul 2010; published 30 Jul 2010

wavelength of the peaks is found to be linearly dependent on the particle size (see the inset). In Fig. 7(b), the extinction efficiencies for three different single particles with axis dimensions of 80, 100 and 120 nm obtained from DDA simulations are given to verify the experimental results.

4.4 The effect of nanoparticle thickness

Another important geometrical parameter affecting the resonance conditions is the thickness of the nanoparticles, which is also a measure of the number of electrons in the system. The LSPR behavior of nanoparticles is known to depend on the diameter-to-thickness ratio, which is called the aspect ratio of the nanoparticle with a cylindrical shape.

To monitor this effect with the thickness variation, two different samples consisting of identical particles with 90 nm diameters but different thicknesses (20 nm and 30 nm) were optically examined by reflectance measurements. As shown in Fig. 8(a), a blueshift in the resonance peak was observed for the thicker sample, which is attributed to the so-called shape factor that appears in analytical solutions to the polarizability for ellipsoidal nanoparticles under a uniform electric field [40,41]. In addition, an increase in the reflectance peak intensity is observed due to the higher metal content on the surface. Figure 8 also shows the DDA simulation results for the same system for comparison. An excellent similarity between the experimental and theoretical results verifies the experimental observation of the reflectance spectra obtained from two samples with different aspect ratios.

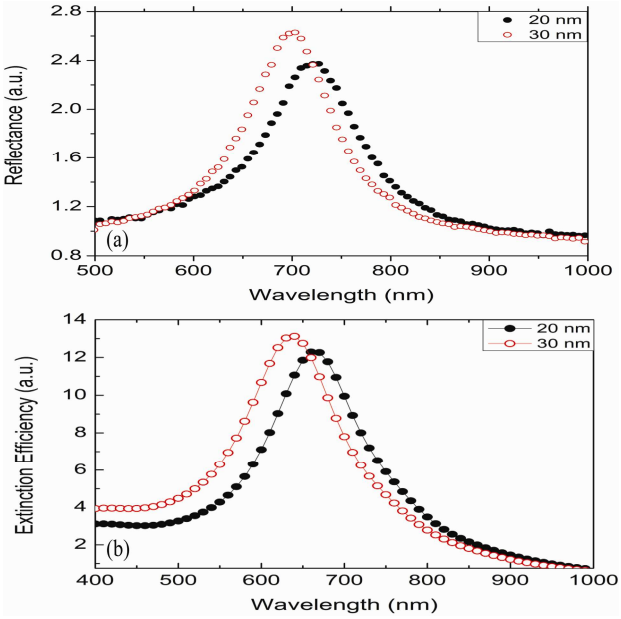

Fig. 8. (a) The reflectance spectra of Au nanoparticles with 90 nm diameter and thicknesses of 20 and 30 nm. (b) The extinction efficiencies obtained for the same particles, located on ITO/air boundary, with DDA calculations.

4.5 The delocalization of surface plasmons

Localized surface plasmon resonances in metal nanoparticles are discussed so far in terms of several parameters. It is interesting to see the limiting condition where the localized behavior of plasmons is lost due to physical contacts among neighboring nanoparticles. Figure 9 presents the reflectance spectra for 30 nm thick Au nanoparticles with varying sizes. It illustrates the transition from localized surface plasmons to surface plasmons. Because the lattice constant of the array is fixed at 200 nm in this sample set, particles with sizes around

#121325 - $15.00 USD Received 5 Jan 2010; revised 8 Jul 2010; accepted 14 Jul 2010; published 30 Jul 2010

this value start to overlap and form large clusters. For the case of particles that are in contact with neighbors, the LSPR peak is seen to disappear. The reflectance for wavelengths larger than a specific value is almost constant, and the threshold value for enhanced reflectance is found to be near 500 nm, which is the plasma wavelength for Au thin film as reported in several experimental studies [42]. The mirror-like behavior of the particle array under normal incident illumination shows the delocalization of the surface plasmons. It is well known that surface plasmon polaritons cannot be excited under normal incidence, and a certain angle of incidence is required to satisfy the wave-vector conservation [43]. It should also be noted that the interstices between the nanoparticle arrays are not uniform in terms of size, shape, position and orientation. The structure presented here is not similar to the system generating well known extra-ordinary transmission peaks reported by Ebbesen et. al. [44].

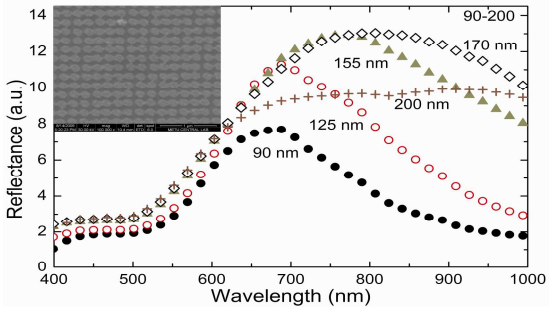

Fig. 9. The reflectance spectra of 30 nm thick Au nanoparticles with varying diameters. The inset shows the SEM image of Au nanoparticles with sizes around 200 nm.

4.6 Intensity modulation with LSPR: a new optical switching method

The multiple peaks observed under unpolarized illumination for particles located with inter-particle distances larger than 200 nm are already mentioned above. Figure 10 shows the reflectance spectra of a Au nanoparticle array with a lattice constant of 400 nm under both linearly polarized and unpolarized illumination. As expected, two separate peaks corresponding to each axis are observed under the unpolarized illumination. Also, for the case of linearly polarized illumination, localized surface plasmons are excited at resonance wavelengths corresponding to the axis that is parallel to the polarized light. The reflectance spectra obtained from each case of illumination show that the intensities are varied depending on the polarization. This behavior of ellipsoidal nanoparticles can be used to design nano-sized optically switched intensity modulators. Considering the sample shown in Fig. 10, illuminating the ellipsoidal nanoparticles with unpolarized pulses having wavelengths of 680 nm, one can modulate the resonance intensity at 780 nm. Thus, the light intensity switching between high and low values can be used as digital pulses to transmit data optically. The variation in the intensity of the LSPR peaks is related to the free electron density of the metal. Because the number of free electrons in a nanoparticle is constant, the intensity of a particular resonance peak depends on whether one or two different polarization axes are excited. To verify that the reflectance intensity is directly related to the free electron density, we can compare the total amount of reflected light for three cases of illumination given in Fig. 10. If the data is integrated between wavelengths of 500 and 1000 nm, where the resonance peaks are located, we obtain the intensity values of 869, 1196 and 1054 for x polarized, y polarized and unpolarized illumination, respectively. When these values are normalized with the axis dimensions to eliminate the variations due to size difference (i.e., surface coverage) the corresponding normalized intensity values are found to be 8.276, 8.248 and 8.432. For this particular example, axis dimensions are taken to be 105 and 145 nm for short and long axis in the case of polarized light and their arithmetic average for the unpolarized light. We see that the normalized intensity is almost the same for three cases. Furthermore, we obtain almost the

#121325 - $15.00 USD Received 5 Jan 2010; revised 8 Jul 2010; accepted 14 Jul 2010; published 30 Jul 2010

same values for all other Au nanoparticle systems with different geometries under the same experimental conditions. This result proves the direct correlation between the amount of reflected light and the electron density in the nanoparticles.

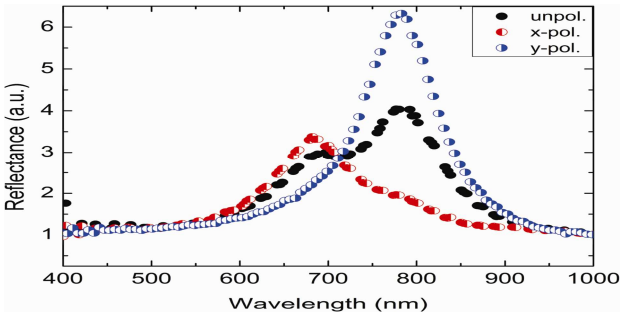

Fig. 10. The reflectance spectra of ellipsoidal Au nanoparticles with axis dimensions of 105 and 145 nm, ordered with a lattice constant of 400 nm. The intensity variations depending on the polarization of the incident light (x and y polarized for short and large axes, respectively) are promising for future nano-sized optically switched intensity modulators.

4.7 Gold vs. silver

The well known solution to the boundary condition problem of a metal sphere under a uniform electric field suggests that the dielectric constant of the metal should be twice the dielectric constant of the host material with a negative sign [45]. Because the host medium is a dielectric, which has a zero imaginary component of the dielectric constant, one should expect a metal with smaller imaginary dielectric constant to have better optical performance. Thus, Ag is expected to provide stronger resonances when compared to Au. Figure 11(a) compares the extinction efficiencies obtained from the DDA calculations for single Au and Ag nanodisks with diameters of 120 nm located on ITO-coated glass. These results confirm that Ag should yield greater reflectance peaks located at shorter wavelengths. With these well-known results, it is widely accepted that Ag nanoparticles should exhibit stronger resonance compared to Au nanoparticles. However, the sulfidation of Ag, which may alter the scattering behavior significantly, is generally overlooked in these considerations. Figure 11(b) gives the reflectance spectra of Au and Ag nanoparticles with identical dimensions. Contrary to the expectations, Ag nanoparticles have a lower scattering yield than Au. In addition, the peak position is shifted to higher wavelengths than the expected values.

The redshift in the LSPR peak and the reduction in intensity are related to the chemical activity of the Ag nanoparticles. The shift of the peak to larger wavelengths is due to the increased effective dielectric constant around the Ag nanoparticles due to the sulfidation. As the metal is sulfidized, the silver sulfide content around the particles increases in time and supersedes the air around the metal nanoparticles [46,47]. The increase in the dielectric constant of the host medium results in a redshift in the resonance peak. Furthermore, the reduced peak intensity can also be attributed to the reduction in the free electron density of Ag as a result of sulfidation. A comparison of the resonance behavior of Ag and Au nanoparticles as a function of time gives a clear picture of the sulfidation effect. Figure 12 shows the reflectance spectra for Au and Ag nanoparticles taken at different time periods. The Au peak is seen to remain almost the same 19 days after the fabrication, while the Ag peak intensity decreases with time significantly and reaches very low values even 8 days after the fabrication. Also, the redshift with sulfidation is clearly seen from the Ag spectra shown in Fig. 12. The effect of sulfidation on the appearance of the Ag nanoparticles can be seen in the SEM image (Fig. 12 inset) taken 30 days after the production of the sample. Detailed discussions on the sulfidation of Ag nanoparticles can be found in the previous studies which employed Auger spectroscopy [46], and energy dispersive spectroscopy [47] techniques to further examine the contamination from sulfur.

#121325 - $15.00 USD Received 5 Jan 2010; revised 8 Jul 2010; accepted 14 Jul 2010; published 30 Jul 2010

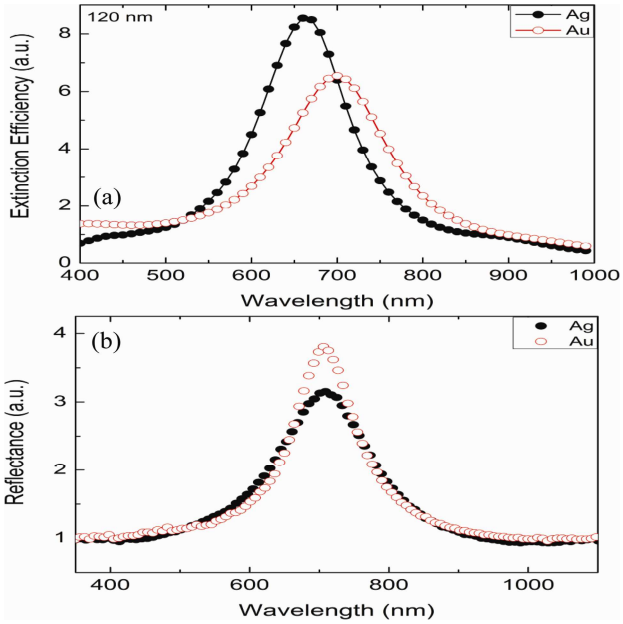

Fig. 11. (a)The extinction efficiencies calculated by DDA for single Au and Ag nanodisks with a 120 nm size located on ITO-coated glass. (b) The reflectance spectra obtained from Au and Ag nanoparticles with equal dimensions located over ITO coated glass.

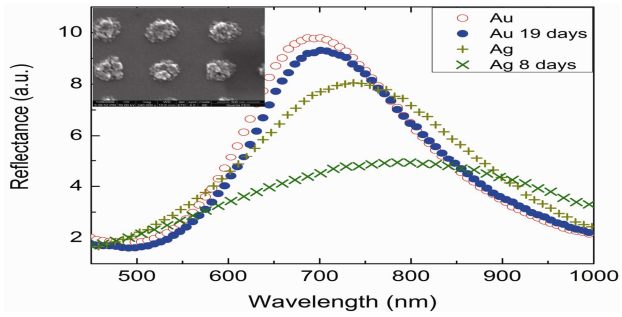

Fig. 12. The reflectance spectra obtained from Au and Ag nanoparticles at different time periods. The Ag peak is altered due to sulfidation. The inset shows the SEM image of Ag nanoparticles taken 30 days after production.

4.8 The size dependence of absorption and scattering cross sections

Finally, the size dependence of the absorption and scattering cross sections of metal nanoparticles is discussed in this section. As already given by Eqs. (1.a) and (1.b), for particles having sizes smaller than a threshold value, the absorption dominates the light-particle interaction. For Ag nanoparticles, a diameter of around 70 nm is found be the threshold value below which the absorption dominates over the scattering. To understand the absorption characteristics, reflectance and transmittance spectra obtained from Ag nanodisks with sizes ranging between 60 and 130 nm were compared. Figure 13 (a) and (b) present the transmittance and reflectance measurements of Ag nanoparticles under unpolarized illumination, respectively.

#121325 - $15.00 USD Received 5 Jan 2010; revised 8 Jul 2010; accepted 14 Jul 2010; published 30 Jul 2010

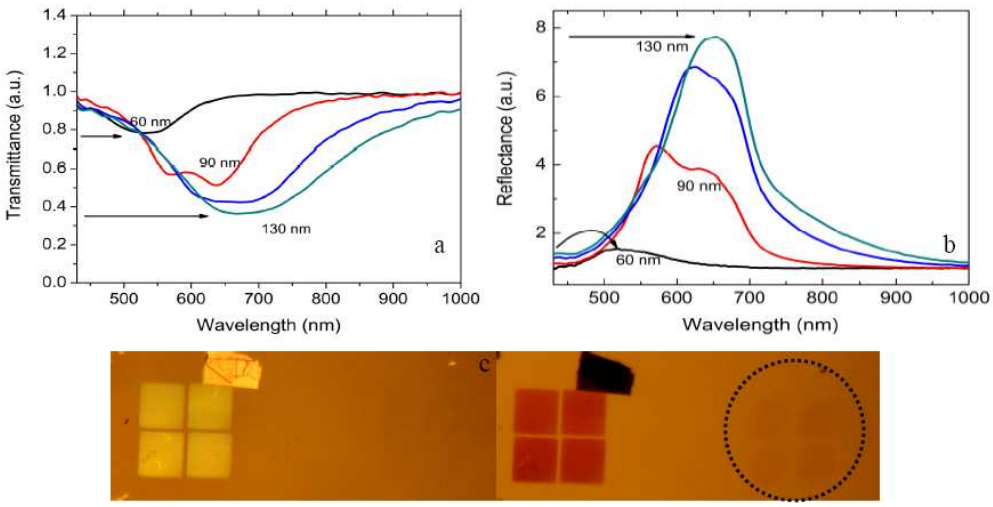

Fig. 13. (a) The transmittance and (b) reflectance spectra of Ag nanoparticles with varying sizes between 60 and 130 nm. The increased ratio of peaks obtained from the 60 and 130 nm particles in transmittance when compared to reflectance measurements can be attributed to the dominant absorption in Ag particles with 60 nm size. (c) The images of 50 and 80 nm particle arrays taken with an optical microscope with reflected (left image) and transmitted light (right image).

In the reflectance spectra, the ratio of the peak values for the 60 and 130 nm particle arrays was around 0.194 (1.5/7.75) while this value was around 0.385 (0.25/0.65) in the case of the transmittance spectra. Because transmittance measurements include the information from both scattering and absorption, it can be concluded that the absorption is more important in particles with 60 nm diameter which is smaller than the 70 nm threshold value. Moreover, a direct observation of the size effect on the absorption is possible by taking the images taken with reflected and transmitted light with an optical microscope. Figure 13 (c) shows the reflected and transmitted light images of Ag particles with 50 and 80 nm sizes. The image of the array consisting of 80 nm particles can be clearly seen in both image types. However, for the case of 50 nm particles, the image of the array cannot be identified with reflected light but can be noticed with transmitted light. Thus, this is a clear observation of the fact that the extinction cross sections of 50 nm Ag disks are dominated by absorption while such a conclusion cannot be drawn for the 80 nm particles, which provide bright images both in the reflection and transmission modes.

The images of arrays taken with an optical microscope were also examined to verify the effects of the size parameters on the LSPR peaks for both front and back illuminations. Figure 14 (a) and (b) present the images of Ag nanoparticle arrays with feature sizes decreasing from the right to left and the lattice constant increasing from the top to bottom with reflected and transmitted light, respectively. In the case of reflection, as the particle size decreases, the color of the array shifts from yellow to green which is a significant blueshift. On the other hand, an increase in the lattice constant results in a reduction in the brightness of the arrays due to the lower surface coverage of the metal. The images taken with transmitted light comprise the unscattered light spectrum where the electron oscillations in particles are not in resonance. Simply varying the size of the particles results in a significant resonance shift, that is visually observable.

#121325 - $15.00 USD Received 5 Jan 2010; revised 8 Jul 2010; accepted 14 Jul 2010; published 30 Jul 2010

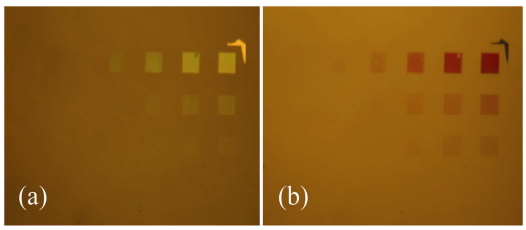

Fig. 14. Images of Ag nanoparticle arrays taken with an optical microscope with (a) reflected light and (b) transmitted light. The particle sizes decrease from right to left, and lattice constants of the arrays increase from the top to bottom.

5. Conclusions

Metal nanoparticles with sizes varying between 50 and 200 nm were fabricated by electron-beam lithography to observe the effects of several geometrical parameters on the localized surface plasmon resonances. Au and Ag nanoparticles were fabricated over a glass substrate with or without ITO films and characterized with reflectance and transmittance measurements. The ITO layer, employed to obtain substrates with higher conductivities, was found to increase the reflected light intensity due to the additional layer introduced into the system. Ellipsoidal nanoparticles with small aspect ratios were found to exhibit single broad peaks under the unpolarized illumination if they were closely located with a lattice constant of 200 nm. In contrast, the reflectance spectra from identical particles with an inter-particle distance of 300 nm resulted in distinct resonance peaks corresponding to the two axes of the ellipsoid. Increasing the lattice constant in particle arrays resulted in the narrowing of the peak and a slight redshift. Thicker nano-disks were found to have larger and blue-shifted peak values. The resonance peaks under linearly polarized illumination showed Lorentzian behavior, verifying the definition of scattering cross section and the almost linear behavior of the dielectric constant of gold in the region of interest. DDA simulations provided effective results, although the limits regarding the accuracy of the approach were slightly violated. Particles with smaller dimensions were shown to have greater absorption cross-sections. Although Ag has promising optical constants, the sulfidation problem of this metal was shown to alter the resonance conditions, and Au was found to be more stable for practical issues. Furthermore, LSPR peaks corresponding to the principal axes in ellipsoidal particles were found to be affected by each other, thus providing promising results for nanometer-scale optically switched intensity modulators.

Acknowledgements

The authors thank Adem Yenisoy for the preparation of self-assembled sample. We also thank Turkish State Planning Organization (SPO) for its financial support for GUNAM project with the contract no: BAP-08-11-DPT-2009-K121030. Partial funding from Scientific and Technological Research Council of Turkey (TUBITAK) is gratefully acknowledged.

#121325 - $15.00 USD Received 5 Jan 2010; revised 8 Jul 2010; accepted 14 Jul 2010; published 30 Jul 2010